Evaluation of Bead-Stiffened Metal Panels

John L. Shideler,* Herman L. Bohon,†
NASA Langley Research Center, Hampton, Va.
and
Bruce E. Greene‡
Boeing Aerospace Co. Seattle, Wash.

Potential weight efficiency for bead-stiffened panels has been demonstrated through fabrication and testing. Theoretically optimum design concepts were identified, and small specimens were tested under combined compression, shear, and bending to determine local buckling failure loads and to verify theory. Large optimized panels were then designed and tested under combined loads. Correlation of test data for large circular tubular panels with theory was conservative and consistent, and indicated reliable and acceptable design theory. Tests of fluted tubular panels indicated general instability failures at loads far below the design values because of nonlinear distortions. Further study of the fluted tubular configuration will be required if its potential weight efficiency is to be attained.

Nomenclature

F_{cy} = compression yield stress
N_x = panel axial compression load
N_{xy} = panel shear load
p = pressure
$\dot{q}$ = heating rate
R_B, R_C, R_S = ratios of actual stress to critical stress for bending, compression, and shear, respectively
T = temperature
t = time
ρ = density

Introduction

FOR the past several years, NASA has been investigating advanced structural concepts which show promise of low structural unit mass in an elevated temperature environment.[1-5] Numerous structural concepts have been studied,[2-4] and some of the most promising are the bead-stiffened panels shown in Fig. 1. This figure[5] shows the critical optimum panel unit mass as a function of compressive load for circular tubular, fluted tubular, fluted single sheet, and skin-stringer designs. The beaded designs are optimized based on combined compression, shear, and bending. The stringer-stiffened design is optimized based on combined compression and bending only. Comparison of the unit mass for optimum conventional stringer-stiffened panels with that for bead-stiffened panels suggests a 25-40% saving in mass over the load range shown. To demonstrate the structural efficiency suggested in Fig. 1, various types of bead-stiffened panels were designed, fabricated, and tested. Particular emphasis was placed on configuration optimization, fabrication techniques, and end-closure joint requirements. Earlier results from the program are reported[6] and detailed documentation is also available.[7-10] This paper presents the correlation of theory with test data from numerous local buckling specimens and large panels. In some cases, analytical methods were modified to achieve improved agreement with test data. Problems which can develop from the use of small specimen test results to predict full-scale panel results are delineated, and the degrading effects of complex failure modes attributed to large prebuckling deformations associated with the flexibility of the thin-walled panels are illustrated.

Presented as Paper 75-815 at the AIAA/ASME/SAE 16th Structures, Structural Dynamics, and Materials Conference, Denver, Colorado, May 27-29, 1975; submitted June 12, 1975; revision received September 18, 1975.

Index categories: Spacecraft Configurational and Structural Design (including Loads); Structural Design, Optimal; Structural Stability Analysis.

*Aerospace Engineer, Thermal Protection Section, Structures and Dynamics Division.

† Head, Thermal Protection Section, Structures and Dynamics Division. Member AIAA.

‡Senior Specialist Engineer, Structural Development and Allowables, Research and Engineering Division. Member AIAA.

Application of Bead-Stiffened Panels

The primary impetus for the study of beaded panels is their application to future hypersonic aircraft and advanced space transportation systems. Recent studies[11] have suggested that exposed wavy surfaces may be aerothermodynamically acceptable when submersed in a relatively thick boundary layer. Consequently, beaded concepts may be applicable to large re-entry vehicles such as the Space Shuttle Orbiter or high-speed vehicles which require heat shields or which operate at high altitudes where a thick boundary layer is present. Further, such configurations are particularly suitable for elevated temperature application because the curved sections permit panel lateral thermal growth without inducing significant stress.

The potential advantage of beaded panel concepts can be best seen with an example illustrated in Fig. 2. In the example, the structural efficiency of optimized stringer-stiffened and circular tubular designs was determined for a typical Shuttle Orbiter re-entry heating profile which is shown in Fig. 2a. Figure 2b shows the insulation thickness required to prevent the primary structure from exceeding a given temperature for the heating profile. In this case, the primary structure was assumed to be covered with metallic heat shields and fibrous

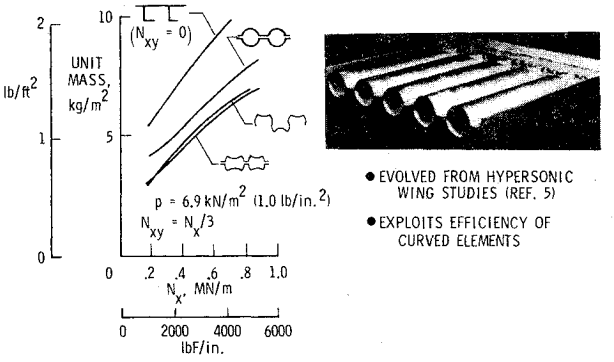

Fig. 1 Potential mass efficiency of bead-stiffened aluminum panels.

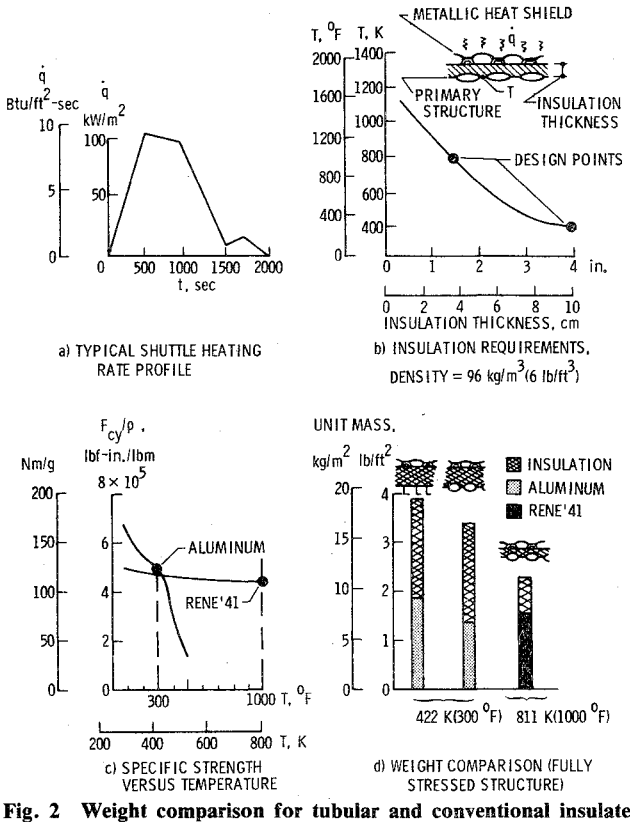

Fig. 2 Weight comparison for tubular and conventional insulated structure exposed to typical shuttle entry.

insulation. To prevent the primary structure from exceeding 811 K (1000°F) requires 3.8 cm (1.5 in.) of insulation, and 10.2 cm (4 in.) are required to reduce that temperature to 422 K (300°F). If the design allowable stress of the primary structure is assumed to vary with temperature as the yield stress varies with temperature, the structural mass predictions from Fig. 1 can be used in conjunction with the specific strength curves for aluminum and Rene 41 in Fig. 2c to determine the structural mass of the three designs shown schematically in Fig. 2d. For this example, a compressive load of 350 kN/m (2000 lb/in.) was used. The insulation requirements for the mass comparisons shown in Fig. 2d were taken from Fig. 2b. The comparisons are made between conventional and beaded panel designs using aluminum as primary structure at 422 K (300°F) and a beaded panel design using Rene 41 at 811 K (1000°F). (These comparisons do not include the mass of the heat shield which was assumed constant for all cases.)

The unit mass comparisons in Fig. 2d show a 15% reduction for the advanced design over the conventional design using aluminum at 422 K (300°F). Using Rene 41 at 811 K (1000°F), a potential of 40% reduction in mass over the conventional design at 422 K (300°F) is indicated.

Program Approach

A study was initiated to assess the mass efficiency of bead-stiffened panels and to develop the design technology required to reliably predict their structural performance. If their potential mass efficiency is to be realized, all failure modes must be identified and properly accounted for in their design. Governing geometric constraint equations were incorporated in a random search type optimization computer program to identify minimum mass designs for several potentially efficient concepts. Three categories of failure modes were considered 1) general instability 2) local instability, 3) material yield. Only failures involving the uniform section of the panel were considered here. Panel end closures, joints, and attachments were assumed to be of sufficient strength to transmit all applied loads to the uniform section. Initial optimum

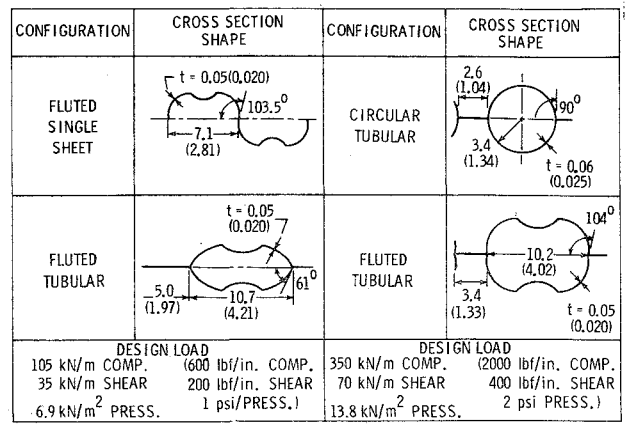

Fig. 3 Configurations selected for 1 m by 1 m (40 in. by 40 in.) panel tests, dimensions in cm (in.).

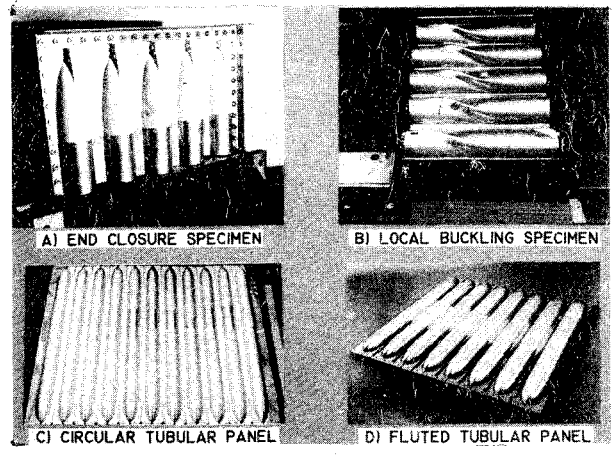

Fig. 4 Test models.

design concepts were subjected to a screening process, which was aided in some cases by preliminary local buckling tests, and which resulted in the selection of the final configurations shown in Fig. 3. The configurations are developed from circular arc elements and flat elements joined in various combinations. They consist of a single sheet fluted design, a circular tubular design, and two fluted tubular designs. The design loads are given in the figure.

Small specimens for the concepts shown in Fig. 3 were fabricated and tested under combined compression, shear, and bending to identify local buckling failure loads, and analytical methods were modified, where necessary, to achieve better agreement with test results. End closure specimens were fabricated and tested to verify the capability to carry specified design loads, but no attempt was made to optimize the end closure designs. Large optimized panels [1 m × 1 m (40 in. × 40 in.)] were then designed and tested under combined loads to determine buckling characteristics for comparison with theory. Only the results for the two configurations shown on the right-hand-side of Fig. 3 (circular tubular and fluted tubular) will be discussed in this paper. Results of the entire study are given in Refs. 7-10.

Test Specimens

To minimize program costs, 7075-T6 aluminum test specimens were used inasmuch as the initial design technology development was independent of material characteristics. Examples of the types of test specimens are shown in Fig. 4. The end closure specimen shown in Fig. 4a and the local buckling specimen shown in Fig. 4b are embedded in a potting material to stabilize the ends and to facilitate attachment to a

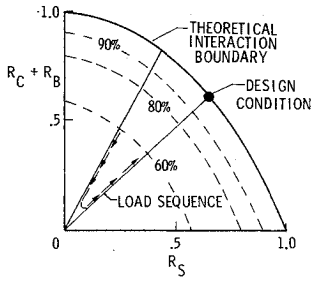

Fig. 5 Test load sequence.

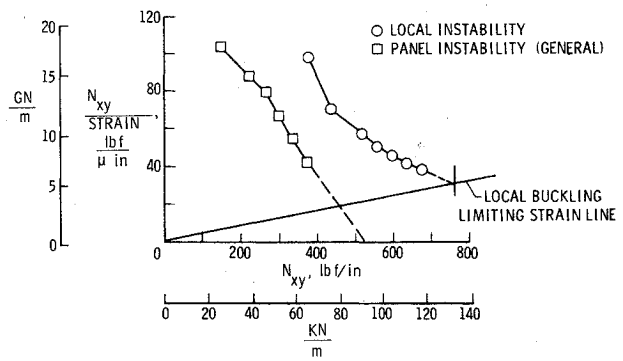

Fig. 6 Force-stiffness nondestructive test method.

loading fixture. Figure 4c shows a 1-m × 1-m (40-in. × 40-in.) circular tubular panel. The panel halves, which were brake-formed,[9] were adhesively bonded together. The panel end closures are reinforced with internal doublers and rivets through the adhesive bond. The fluted tubular panel shown in Fig. 4d has both external and internal doublers. The rivets in the fluted tubes, visible at discrete locations along the tube length, fasten inserts inside the tube. These inserts are discussed in a later section.

Test Technique

Panels and small specimens were tested in combined load test fixtures designed and fabricated for this study. The test fixtures were capable of applying compression, shear, and bending either separately or in combination. Extensive finite-element analyses were conducted to support the design of edge members, joints, buffer bays, and loading plates to minimize the undesirable influences of the boundary members upon the stress distributions within the test panel.

The load sequence used to test the panels is indicated in Fig. 5 where R_C,R_B, and R_S are ratios of actual stress to theoretical failure stress for compression, bending, and shear, respectively. The interaction curve is a theoretical failure curve for combined load, and the point on the curve designates the panel design condition. This design point corresponds to a load condition of 350 kN/m (2000 lb/in.) compression, 70 kN/m (400 lb/in.) shear, and 13.8 kN/m^2 (2 psi) lateral pressure. The radial lines on Fig. 5 indicate several of the 10 different combinations of compression, shear, and bending load under which the panels were tested. A nondestructive test technique referred to as the force-stiffness method (a technique based on strain measurements)[12] was used to obtain failure predictions from a single panel at all 10 load combinations. The arrows on the figure illustrate the load sequence. Load is increased under a selected load condition until a preselected level is reached (60% of theoretical failure load for the illustration shown) at which time a force-stiffness prediction of failure may be made. Load is then removed, and the panel is loaded in a second load combination to the same preselected level. The procedure is continued until the panel has been loaded in all 10 combinations of load and force-stiffness predictions have been made in all 10 conditions. The process is then repeated to higher load levels (80% and then

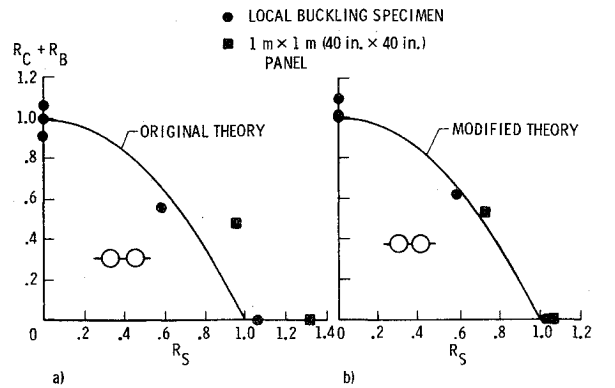

Fig. 7 Circular tubular local buckling results (bead crippling): a) local buckling specimen and panel failures compared to original theory; b) local buckling specimen and panel failures compared to modified theory.

90% of theory for the case illustrated in Fig. 5) where more accurate force-stiffness predictions of failure loads can be made. The degree of repeatability of the force-stiffness test data indicate if any prior damage has occurred in the panel. In this manner, test data can be obtained over the entire range of loading conditions with minimum risk of panel failure. After the failure interaction curve was determined nondestructively, the panel was loaded to failure in one of the 10 load condition to provide a check point for the force-stiffness prediction.

An illustration of the force-stiffness method is shown in Fig. 6. This example is for the panel loaded in shear only, but the principle is the same for other loading conditions. A stiffness parameter obtained by dividing the applied load N_{xy} by the measured strain is plotted against the applied load. The symbols indicate load levels where strain and load data were recorded. The two curves are for two different modes of failure, one for general instability, shown by the squares, and one for local buckling shown by the circles. Extrapolation of the data shown by the squares to the horizontal axis gives a prediction of the failure load on general instability. In this case, the strain measurement used is the difference between two strain gages located on opposite crests of a tube in the central region of the panel. Thus, the strain measurement is sensitive to bending deformations of the panel which are associated with the fundametal general instability failure mode. The prediction of local buckling is obtained by extrapolating the data based on local strain measurements to a limiting strain line. This line of constant strain is the strain level at which local failure is expected to occur and was determined experimentally for each concept during tests of the small local buckling specimens. The strain measurements used for force-stiffness prediction of local buckling of the large panels were obtained from strain gages mounted in locations where high strain was expected, usually at the crest of a tube. Successful application of the force-stiffness method depends on the proper location of strain gages to measure the strain associated with particular expected failure mode shapes. Numerous force-stiffness plots (usually about 10 or 12) were constructed during each test using those strain measurements which were judged most likely to detect the expected failure modes.

Correlation of Test Data With Theory

Three types of specimens of the circular tubular and fluted tubular designs were tested. The types include local buckling, end closure, and 1 m × 1 m (40 in. × 40 in.) panel specimens. As noted earlier, end closure designs were not optimized in this program, and their strength requirements were verified through specimen tests. All end closure and local buckling specimens were tested to failure. Thus, the number of failure points for these tests is identical to the number of test specimens. However, as many as 10 predicted failure points

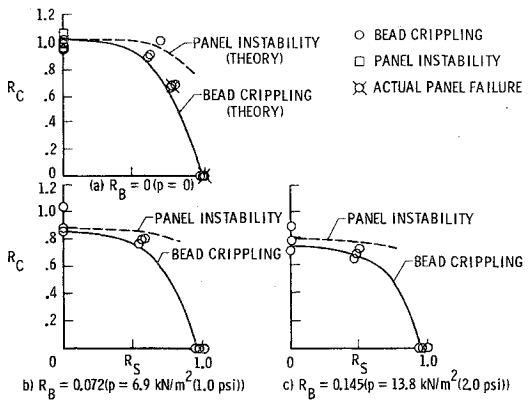

Fig. 8 Circular tubular panel test results compared to modified theory (*F/S* test data except where noted; R_C, R_S, and R_B are based on load, not stress).

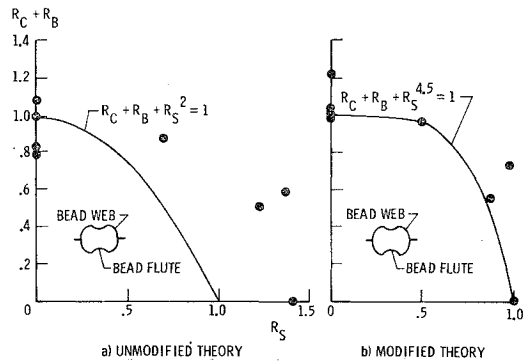

Fig. 9 Fluted tubular local buckling test results (bead web crippling).

were obtained for each 1 m × 1 m (40 in. × 40 in.) test panel through the use of the force-stiffness nondestructive test technique.

Circular Tubular Configuration

Local buckling test results for the circular tubular configuration are compared with theoretical interaction curves shown in Fig. 7. Failure test data are shown for five local buckling specimens and also for two full-size panels which failed in local buckling. All test data and theory are for failure of the circular arc (bead crippling).

The interaction curve shown in Fig. 7a is based on the original theory used to design the configuration. The small specimen test results (circular symbols) indicate that theory may be slightly unconservative, but no attempt was made to modify the design theory prior to designing and testing the large panels. However, results from two large panels tested to failure (shown by square symbols in Fig. 7a indicate that the theory is conservative in shear, and is conservative by a large margin. Thus, theory which accurately predicted the failure loads of the small specimens, as verified by the test results, did not accurately predict failure loads of the large panels.

Correlation of these data indicated that a modification to the length effect for determining the local buckling coefficient in shear, combined with a knock-down factor of 0.9 for local buckling in compression resulted in reasonably good agreement. The result of these modifications to the theory is a much improved comparison as is reflected in Fig. 7b where the local buckling specimen and large panel failure data are compared with an interaction curve based on the modified theory. A more descriptive discussion of the modification to the local buckling equation is given in Ref. 8.

All results of the large panel tests are given in Fig. 8 for normal pressure loads of 0, 6.9, and 13.8 kN/m^2 (0, 1, and 2 psi). The actual panel failure points are noted by crossed symbols; all other data points were determined by the force-stiffness

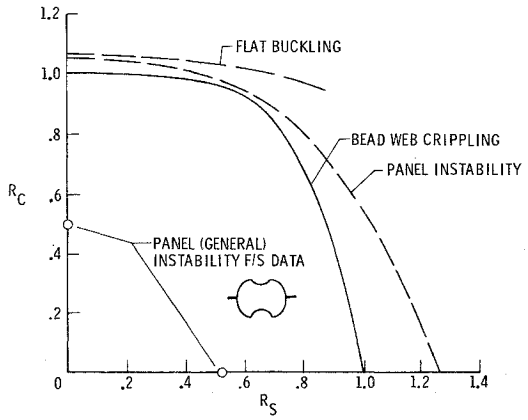

Fig. 10 Fluted tubular panel test data compared with modified theory ($p = 0$).

nondestructive testing method. The circular symbols denote bead crippling, and the square symbols denote panel instability. The two curves shown are based on modified theory where the failure mode is either bead crippling (solid curve) or panel general instability (dashed curve) determined by assuming the panel to be a simply supported wide column. The test data are shown for the 10 loading conditions under which the panels were tested, and were obtained from three essentially identical panels.

General instability failures were detected only in pure compression where theory indicates either local or general instability may occur. The slightly unconservative data points shown for pure compression (Fig. 8a) may result from a deficient end closure which was only marginally satisfactory in pure compression. Correlation factors for each data point were determined by dividing each test value by the value predicted by theory. The average correlation factor for these data was 1.035 indicating that the test data were very consistent and that theory is generally conservative as can be seen from Fig. 8. Thus, it is believed that the theory (as modified) used to predict the behavior of the circular tubular panel configuration is acceptable for design purposes. The theory and the associated modifications are presented in detail in Ref. 8.

Fluted Tubular Configuration

Local buckling test data from small specimens of the fluted tubular concept are shown in Fig. 9a compared with interaction curves based on the original theory used to design the specimens. As can be seen, the theory appears to be very conservative in shear and unconservative in compression. Based on the results shown in Fig. 9a, the local buckling theory was modified to achieve the better agreement shown in Fig. 9b. Three modifications were made, 1) a knock-down factor of 0.80 was applied to the failure equation for bead web crippling in compression, 2) a factor of 1.40 was applied to the failure equation for bead web crippling in shear, and 3) the shape of the interaction equation was modified by changing the exponent on R_S from 2 to 4.5.

When the first full-scale fluted tubular panel was tested, force-stiffness test results indicated general instability failures in compression and in shear at loads far below the values predicted by the modified theory. Figure 10 shows these data points compared with the interaction curves for bead web crippling, general instability, and flat buckling. Although bead web crippling is the predicted failure mode, there was no evidence of web crippling indicated by the tests. (Buckling of the flats was not expected, as indicated by the curve in the figure, nor was it evidenced by the tests.) The degradation of panel performance and the change in failure mode was attributed to large deformations of the cross section which occurred during the tests. The typical deformation under compression and pressure load is shown in Fig. 11a. The panel deformation resembles a general instability mode resulting in

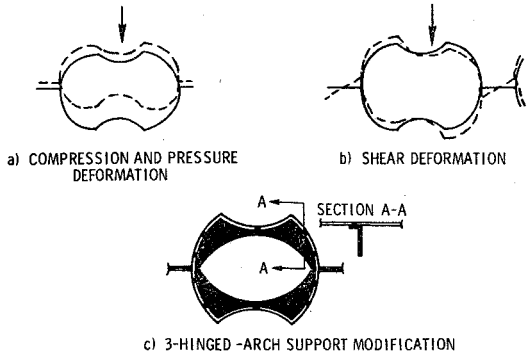

Fig. 11 Panel deformations and tube modification.

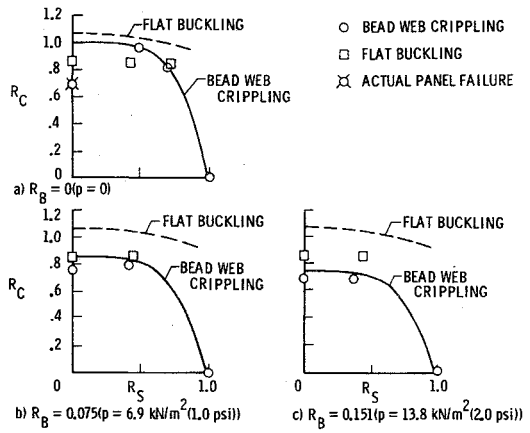

Fig. 12 Comparison of panel test results with modified theory for fluted tubular panel with three-hinged-arch support (F/S test data except where noted; R_C, R_S, and R_B are based on load, not stress).

a flattening of the cross section (Brazier effect).[13] This tube flattening caused a reduction in section stiffness. In Fig. 11b tube rotations and distortions which occur under shear load are illustrated. It appears that in addition to rotation of the tubes, a local distortion of the bead web radius occurs.

To suppress these large deformations and therby improve the performance of the fluted tubular panels, several types of tube inserts were considered. The most successful of these, a three-hinged-arch support, is shown in Fig. 11c. The support (see Sec. A-A) is an angle which forms a partial bulkhead in the tube, stiffens the circular arc elements to prevent local changes in radius, but still allows thermal growth in the transverse direction. Each half-support is riveted into a panel half at approximately 4-in. spacing prior to the panel halves being assembled. The addition of the inserts results in an increase in unit mass of about 10%.

Test results for the modified panel are shown in Fig. 12. The curves shown are obtained from modified theory based on local buckling test data; see Fig. 9b. The symbols are force-stiffness predictions for failure in bead web crippling (circular symbols) and in flat buckling (square symbols). Even though the force-stiffness predicted data show good agreement with bead web crippling theory, actual failure of the panel, shown by the circular crossed symbol in Fig. 12a, occurred in compression at only 69% of theory. Prior to panel failure, square Moire fringe patterns were observed in the flats near the end closures which indicates buckling of the flats. As the load was increased, additional square Moire patterns appeared closer to the panel center. Consequently, early failure in what appears to be bead web crippling may have been precipitated by flat buckling. As a result, the force-stiffness data shown in Fig. 12 cannot be considered reliable because the data were affected by complex modal behavior and possible interaction between failure modes. (Application of the force-stiffness method is dependent on proper identification of the failure

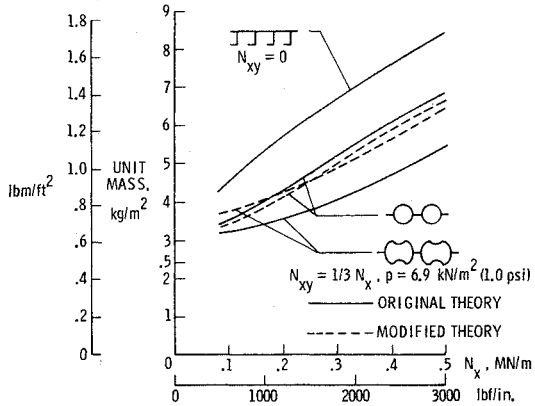

Fig. 13 Improved weight-strength curves for 1 m by 1 m (40 in. by 40 in.) aluminum panels (excluding end closure/attachment weights).

mode.)[12] Thus, it appears that although the inserts suppressed the general instability mode of failure, they did not adequately prevent distortion of the fluted tube. It is therefore apparent that extensive analytical and experimental study of the fluted tubular configuration will be required if its potential structural efficiency is to be attained.

Improved Mass-Strength Predictions

The mass efficiency for both the circular tubular and fluted tubular panel concepts are shown in Fig. 13 for the original theory (solid line) and for the theory modified on the basis of test results discussed herein (dashed line). The curves are for a combined loading condition of compression, shear (a shear/compression ratio of ⅓), and lateral pressure [6.9 kN/m^2 (1.0 psi)] and do not include end closure or attachment weights. The increase in mass shown by the dashed line for the fluted configuration has been estimated since no satisfactory correlation between theory and test values was achieved. Based on the 10% mass penalty for the inserts, and on the actual panel failure load which was less than predicted (Fig. 12a), the curve for modified theory was determined to be 20% higher than the curve for original theory.

The modified mass-strength curve for the circular tubular panel is based on theory used to determine the interaction curves shown in Fig. 8 and results in a 5% reduction in mass when compared to the original theory. As previously mentioned, the modified theory for the circular tubular panel provides a reliable basis for design in the load range studied. Comparison of the mass-strength curve for the circular tubular panel with that for an optimized stringer-stiffened panel (optimized for compression and pressure only)[14] indicates an available mass savings of about 25%.

Comparison of the two dashed lines in Fig. 13 leads to the conclusion that the circular tubular configuration and the fluted tubular configuration exhibit about the same structural efficiency. However, a comparison on the basis of consistent, predictable performance results in the circular tubular configuration being clearly superior.

Conclusions and Recommendations

A program has been conducted to develop design technology for bead-stiffened panels applicable to hypersonic aircraft and advanced space transportation systems. To verify the theoretical mass efficiency of these panels, several optimized panels were designed, fabricated, and tested. The circular tubular concept proved to be highly efficient and its performance can be reliably predicted. However, tests of the fluted-tubular concept identified complex failure modes which jeopardize its potential efficiency.

Test data from local buckling specimens of the circular tubular and fluted tubular concepts clearly illustrated the problems that can occur from relying on small specimens to

predict full-scale results. Failure modes of the fluted tubes which cannot be accounted for by small deflection theory were not evident in tests of the local buckling specimens; these modes were present, however, in the full-scale panel tests, and they greatly reduced load capability of the panel. To further improve the efficiency of beaded panels, a detailed stress analysis of panel closeouts should be conducted to improve the load path and to reduce parasitic mass.

Finally, it is desirable to demonstrate the applicability of beaded panels to an elevated temperature environment using high-temperature alloys. Such a demonstration may be accomplished by tests planned at the NASA Dryden Flight Reseach Center where a large hypersonic wing test structure has been designed and fabricated under contract[15] to meet aerothermal requirements of a hypothetical aircraft. Circular tubular panels have been fabricated from Rene 41 for installation in this fixture which will be subjected to temperatures of 1006 K (1350°F) and to simulated aerodynamic loads representative of hypersonic flight. Performance will be correlated with theory and compared with results at ambient tempratures. Results from this program should reveal the suitability of bead-stiffened panels for applications at elevated temperatures.

References

[1]Heldenfels, R.R., "Structural Prospects for Hypersonic Air Vehicles," ICAS Paper 66-31, Sept. 1966.

[2]Shideler, J.L. and Jackson, L.R., "Fuselage and Tank Structures for Hypersonic Aircraft," NASA SP-148, 1967.

[3]Anderson, MS., Robinson, J.C., and Klich, G.F., "Analysis of Wing Structures for Hypersonic Aircraft," NASA SP-148, 1967.

[4]Plank, P.P., Sakata, I.F., Davis, G.W., and Richie, C.C., "Hypersonic Cruise Vehicle Wing Structure Evaluation," NASA CR-1568, May 1974.

[5]Card, M.F., Davis, J.G., and Shideler, J.L., "Advanced Design Concepts for Shuttle Airframe Structures," NASA TM X-2570, 1972.

[6]Musgrove, MD., Greene, B.E., Shideler, J.L., and Bohon, H.L., "Advanced Beaded and Tubular Structural Panels," *Journal of Aircraft*, Vol. 11, Feb. 1974, pp. 68-75.

[7]Musgrove, M.D. and Greene, B.E., "Advanced Beaded and Tubular Structural Panels, Summary Document," NASA CR-2514, 1975.

[8]Greene, B.E., "Substantiation Data for Advanced Beaded and Tubular Structural Panels, Volume 1, Design and Analysis," NASA CR-132460, 1975.

[9]Musgrove, M.D. and Northrup, R.F., "Substantiation Data for Advanced Beaded and Tubular Structural Panels, Volume 2, Fabrication," NASA CR-132482, 1975.

[10]Hedges, P.C. and Greene, B.E., "Substantiation Data for Advanced Beaded and Tubular Structural Panels, Volume 3, Testing," NASA CR-132515, 1975.

[11]Brandon, H.J., Masek, R.V., and Dunavant, J.C., "Aerodynamic Heating to Corrugation Stiffened Structures in Thick Turbulent Boundary Layers," *AIAA Journal*, Vol. 13, Nov. 1975, pp. 1460-1466.

[12]Jones, R.E. and Greene, B.E., "The Force/Stiffness Technique for Nondestructive Buckling Testing," *Journal of Aircraft*, to be published.

[13]Brazier, L.G., "On the Flexure of Thin Cylindrical Shells and Other 'Thin' Sections," *Proceedings of the Royal Soc.*, Series A, Vol. CXVI, 1926, pp. 104-114.

[14]Giles, G.L. and Anderson, M.S., "Effects of Eccentricities and Lateral Pressure on the Design of Stiffened Compression Panels," NASA TN D-6784, 1972.

[15]Plank, P.P. and Penning, F.A., "Hypersonic Wing Test Structure Design, Analysis, and Fabrication," NASA CR-127490, 1973.